

Tornillos modeled as self-oscillations of fluid filling a cavity: Application to the 1992–1993 activity at Galeras volcano, Colombia



K.I. Konstantinou*

Dept of Earth Sciences, National Central University, Jhongli 320, Taiwan

ARTICLE INFO

Article history:

Received 28 July 2014

Received in revised form 14 October 2014

Accepted 31 October 2014

Available online 8 November 2014

Keywords:

Tornillos
Galeras
Cavity
Dome
Self-oscillation

ABSTRACT

Tornillos are quasi-monochromatic seismic signals with a slowly decaying coda that are observed near active volcanoes and geothermal areas worldwide. In this work a lumped parameter model describing the tornillo source process as the self-oscillations of fluid filling a cavity is investigated. A nonlinear ordinary differential equation is derived that governs the behavior of the model taking into account viscous and nonlinear damping as well as the reaction force of the fluid inside the cavity. This equation is numerically integrated both for different cavity sizes and different fluids of volcanological interest, such as gas ($\text{H}_2\text{O} + \text{CO}_2$, $\text{H}_2\text{O} + \text{SO}_2$) and gas-particle mixtures (ash- SO_2 , water droplets- H_2O). This cavity model predicts that when the filling fluid is a mixture of ash and SO_2 the signal duration will increase until the mixture becomes enriched in ash and then the duration exhibits a decrease. Additionally, the damping coefficients ($=1/2Q$) of the synthetic signals are estimated in the range between 0.002 and 0.014. Both results agree well with the temporal variation of tornillos duration and the estimated Q quality factors/damping coefficients observed at Galeras volcano. In the context of the cavity model, tornillo frequency variations from 4 Hz to 1 Hz observed prior to eruptions can be interpreted as the result of fluid composition changes as more ash particles are added. This is in agreement with the observation that gas accumulation at Galeras was a steady rather than an episodic process and that tornillos were most likely triggered after a fluid pressure threshold had been exceeded.

© 2014 Elsevier B.V. All rights reserved.

1. Introduction

Tornillos represent an enigmatic class of quasi-monochromatic seismic signals with an extended coda that are observed near active volcanoes and geothermal areas. Such signals are quite distinct from the usual long-period events that are also observed at volcanoes but have shorter coda and may also contain more frequencies. The word ‘tornillo’ is the Spanish word for screw and was used to describe extended coda signals recorded during the 1992–1993 eruption of Galeras volcano, Colombia. The choice of this word was motivated by the resemblance of these signals with the profile of a screw thread (Narváez et al., 1997) (Fig. 1). Even though similar events with slowly decaying coda have been recognized previously in a number of Japanese volcanoes (Hamada et al., 1976), the observations made at Galeras were the first detailed ones resulting in the identification of 13 different types of tornillos. These observations were prompted by the fact that ash eruptions at Galeras were almost always preceded by such signals highlighting their potential value for eruption forecasting (Narváez et al.,

1997; Gómez and Torres, 1997; Gómez et al., 1999; Seidl et al., 1999). Tornillo events have been reported ever since in several other volcanoes worldwide including Kelut in Indonesia (Lesage and Surono, 1995), Tongariro in New Zealand (Hagerty and Benites, 2003), Mt Griggs in Alaska (De Angelis, 2006) and Vulcano in Italy (Milluzzo et al., 2010) among others.

The extended coda of the tornillo signals has been found to span in duration from few tens to hundreds of seconds while systematic variations in their duration were observed before ash eruptions at Galeras. Observed dominant frequencies are the same at all recording stations, a characteristic which suggests that these frequencies reflect a source effect. A less mentioned characteristic of these signals is their relatively small amplitude that limits the maximum distance at which they can be clearly observed to about 4 km or less (Table 1). Additionally, amplitude modulation has been frequently observed in tornillo signals and it can be explained either as the superposition of two close eigenfrequencies of a resonator source, or the superposition to the signal of noise having very similar frequency (see Milluzzo et al. (2010)). In general, the tornillo frequency content lies in the band between 1 and 16 Hz exhibiting either a single-frequency peak spectrum or multiple peaks that are usually not part of a harmonic series. Efforts to locate the tornillo

* Fax: +886 3 4222044.

E-mail address: kkonst@ncu.edu.tw

source have used traditional travel-time inversion methods when the signal had an impulsive onset (Molina et al., 2004), as well as waveform modeling techniques (Kumagai et al., 2002; Nakano et al., 2003). In most cases the source was located near the main eruptive crater of each volcano at a depth range of a few hundred meters.

One model that has been often used for explaining the source properties of long-period events and tornillos is that of the resonating fluid-filled crack (Chouet, 1996 and references therein). In this model resonance is induced by a pressure transient applied over a small area of the crack wall and the modes that are excited depend on factors such as the extent of the crack surface, time history of the transient and boundary conditions. More importantly, the crack model predicts that long-lasting oscillations of the crack are possible when there is a large impedance contrast between the fluid and the solid implying the presence of high gas content. Several studies that have measured quality factors for tornillo events have explained the large values obtained (>100) based on the crack model predictions, invoking a fluid composition that consists of gas and ash/liquid particles (Kumagai et al., 2002; Hagerty and Benites, 2003; Molina et al., 2004; Nakano and Kumagai, 2005; Milluzzo et al., 2010; Alparone et al., 2010). On the other hand, Seidl and Hellweg (2003) argued that tremor and tremor-like signals (such as tornillos) do not provide a window into the volcano conduit system, but rather illuminate small elementary volumes where oscillatory fluid movement takes place. The authors suggested a physical model based on the free vibrations of a fluid-filled cavity excited by a pressure pulse. However, their analysis only considered a linearized version of the model and investigated its behavior only for a particular case of steam-CO₂ mixture.

In this work, the fluid-filled cavity model for tornillo excitation is re-examined by incorporating nonlinear effects and investigating the characteristics of the excited acoustic oscillations. First, a description of the general properties of this cavity oscillator is given followed by the identification of two nonlinear effects, namely nonlinear damping and the reaction force of the fluid inside the cavity. The ordinary differential equation describing this lumped parameter model is integrated numerically utilizing different cavity sizes and fluid types. The characteristics of the cavity model oscillations (duration, frequency, quality factors, reduced displacement) are then compared to those of tornillos at Galeras in order to see to what extent they can reproduce the observations.

Finally, the discussion focuses on the issue whether the cavity model has a physical basis that is supported by observations at Galeras but also at other volcanoes where tornillos have been observed.

2. The fluid-filled cavity oscillator

2.1. General properties

A cavity oscillator (also known as Helmholtz oscillator) is a tube-cavity system where a slug of fluid inside the tube moves in an oscillatory motion (Fig. 2). It should be noted that the word ‘slug’ is used in this work not to describe a large gas bubble as is usually done in volcanological studies, but just to denote the quantity of fluid residing in the tube. For simplicity the cavity is here represented having a cylindrical shape with radius R and height h , connected to a tube that has length L and radius r . When the linear dimension of the oscillator is much smaller than the oscillation wavelength, two assumptions can be made: (a) the pressure inside the cavity is spatially uniform, and (b) the slug of fluid in the tube moves in phase as a whole. Under these assumptions the oscillator system can be considered as a compact source where the pressure inside the cavity is everywhere the same and the approximation of incompressible fluid flow can be applied (Rienstra and Hirschberg, 2004).

The cavity oscillator is subject to energy dissipation in the form of viscous losses due to the movement of fluid near the walls of the tube. The dissipation can be quantified by use of the damping coefficient δ in which case the viscous force will be equal to $2\delta m\dot{x}$ where m is the mass of the slug of fluid in the tube and \dot{x} its velocity. Howe (1976) developed the theory of excitation of a fluid-filled cavity by external disturbances that were located arbitrarily close to the orifice of the tube. The author found that the damping coefficient due to viscous losses can be approximated as

$$\delta = \frac{\sqrt{\omega_0}}{r\sqrt{2}} [\sqrt{\nu} + \sqrt{\kappa}(\gamma - 1)] \quad (1)$$

where γ is the specific heat ratio of the fluid, ν its dynamic viscosity in m²/s, κ is the thermometric conductivity defined as $\kappa = k/\rho_f c_p$ with k being the thermal conductivity of the fluid, ρ_f its density and c_p its specific heat under constant pressure. The quantity ω_0 symbolizes the natural frequency of the fluid-filled cavity, given by

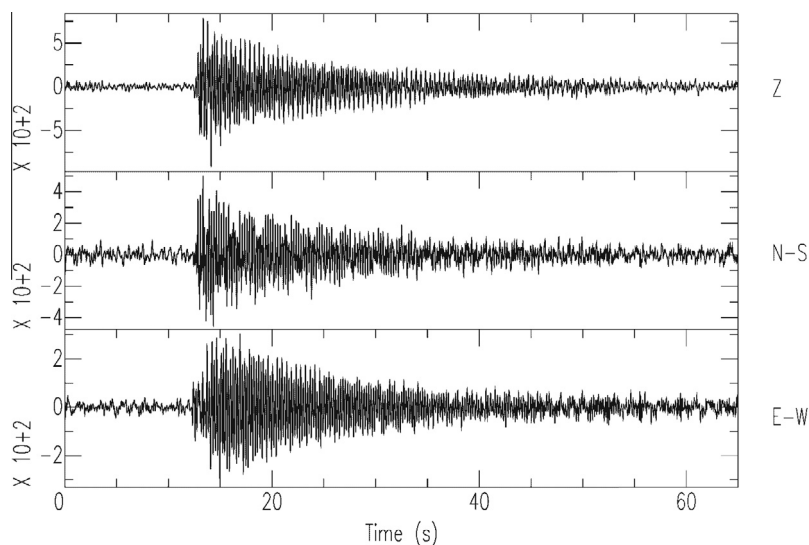


Fig. 1. Velocity waveforms of a tornillo event recorded by a three component short-period sensor installed at the area of the Tatun Volcano Group, northern Taiwan. Amplitudes are in arbitrary units.

Table 1

List of stations distance from the active craters where tornillos were observed (d_{obs}) and distances of the furthest station (d_{max}) where the tornillo signal was either not recorded at all or signal-to-noise ratio was very small. The column f signifies the range of dominant tornillo frequencies at each volcano.

Volcano	Region	d_{obs} (km)	d_{max} (km)	f (Hz)	Reference
Kelut	Indonesia	0.5	7	5–6	Lesage and Surono (1995)
Galeras	Colombia	4	5	0.9–3.5	Gómez and Torres (1997)
Tongariro	New Zealand	2.5	7	1.2–3.8	Hagerty and Benites (2003)
Mt Griggs	Alaska	4	7	2.5	De Angelis (2006)
Vulcano	Italy	0.5	2	4–16	Milluzzo et al. (2010)

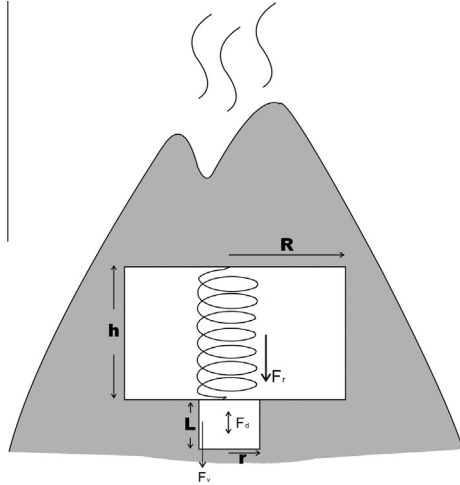


Fig. 2. Cartoon illustrating the geometry of the cylindrical tube-cavity oscillator. The cavity has a height h and a radius R while its cross-section is $S = \pi R^2$. The tube has a length L and radius r while its cross-section is equal to $s = \pi r^2$. The mechanical analog of this oscillator is also shown as a spring (fluid inside the cavity) and an attached mass (fluid slug in the tube) while viscous losses exist near the walls of the tube. Also shown are the forces involved, namely F_r the reaction force of the fluid inside the cavity, F_v the viscous force near the walls and F_d the nonlinear damping force exerted on the fluid in the tube.

$$\omega_0 = c\sqrt{\frac{s}{L_e V}} \quad (2)$$

where c is the speed of sound for the fluid, s is the cross-section of the tube, V is the volume of the cavity and L_e is a quantity termed as 'effective length' that is equal to (Rienstra and Hirschberg, 2004)

$$L_e = L + \frac{16r}{3\pi} \quad (3)$$

The physical meaning of the effective length stems from the inertia of the acoustic flow at both ends of the tube, in the sense that the slug moves within a length that is larger than the length L of the tube. The term $16r/3\pi$ is therefore an appropriate correction added to the original length value.

2.2. Nonlinear effects

The mechanical analog of the fluid-filled cavity is that of a mass suspended from a spring, where the mass represents the fluid slug and the spring corresponds to the fluid residing within the cavity (cf. Fig. 2). In every cycle of oscillation the fluid in the cavity works as an elastic spring pushing the slug towards the tube. The elastic properties of the cavity fluid can be calculated after its thermodynamic state is considered, as described by changes in pressure and volume variables. Assuming that the process is adiabatic and P_0 is the initial fluid pressure in the cavity, then the relative change of pressure P due to a small displacement x of the slug can be expressed as a series expansion (Boullousa and Bustamante, 1992)

$$\frac{\Delta P}{P_0} = -\left[\gamma \frac{sx}{V} - \frac{1}{2}\gamma(\gamma+1)\left(\frac{sx}{V}\right)^2 + \dots\right] \quad (4)$$

Taking into account that $P_0 = \rho_f c^2 / \gamma$ the reaction force F_r exerted by the cavity fluid on the slug can be written as

$$F_r = \Delta P s = -\left(\frac{\rho_f c^2 s^2}{V}\right) \left[x - \frac{1}{2}(\gamma+1)\left(\frac{s}{V}\right)x^2 + \dots\right] \quad (5)$$

The previous equation shows that the reaction force is a nonlinear function of the slug displacement x . The coefficient of the nonlinear term is inversely proportional to the volume V , therefore it will become more significant for smaller cavities.

Another effect that has to be considered is that of variations in mechanical energy once the configuration of the flow is sharply changed. This occurs in the cavity oscillator since the fluid moves from a smaller conduit cross-section to a larger one and vice versa. The dynamic pressure of the fluid can give a measure of this effect and it may be expressed through a formula given by (Batchelor, 1967)

$$\Delta p = \frac{1}{2}\rho_f \dot{x}^2 \left(1 - \frac{S}{s}\right)^2 \quad (6)$$

where S is the cross-section area of the cavity. If Δp is multiplied by the cross-section of the tube, the corresponding force that is every time exerted on the slug can be obtained

$$F_d = \Delta p s = \left(\frac{1}{2}\rho_f \zeta s\right) \dot{x}^2 \quad (7)$$

where the expression $\left(1 - \frac{S}{s}\right)^2$ has been replaced by the variable ζ . This force depends on the velocity of the slug therefore it can be characterized as a damping force. Furthermore, since it is expressed as a nonlinear function of \dot{x} hereafter it will be referred to as 'nonlinear damping' to distinguish it from the linear one. Nonlinear damping reflects increases and decreases of dynamic pressure as the fluid slug gains or loses kinetic energy.

2.3. Governing equation and self-oscillation mechanism

The equation of motion for the tube-cavity oscillator is derived in Appendix A and the nonlinear ordinary differential equation that is obtained is

$$\ddot{x} + 2\delta\dot{x} + \frac{\zeta}{2L_e}|\dot{x}|\dot{x} + \frac{c^2 s}{L_e V} \left[x - \frac{1}{2}(\gamma+1)\left(\frac{s}{V}\right)x^2\right] = 0 \quad (8)$$

where \ddot{x} is acceleration and the quantity $c^2 s / L_e V$ is equal to the square of the natural frequency of the oscillator (ω_0^2). While linear damping is always related to energy dissipation due to viscous losses, nonlinear damping may be related to either energy loss or gain as mentioned previously. For this reason the slug velocity in the nonlinear damping term has been substituted by the product $|\dot{x}|\dot{x}$ so as to take into account the sign of the velocity. Nonlinear damping will become positive when the fluid moves from the tube towards the cavity. In this case the slug is doing work against the pressure gradient and therefore loses energy. When the reaction force pushes the slug towards the tube its kinetic energy increases

again and the nonlinear damping becomes negative. At this instance, the pressure inside the cavity becomes lower whereas near the orifice it becomes higher and the slug moves back towards the cavity starting a new cycle of oscillation.

The equation of motion is formulated as a homogeneous ordinary differential equation since the oscillatory motion of the slug is not regulated by some external driving force, but rather synchronizes with the reaction force of the fluid inside the cavity. The term ‘self-oscillation’ can be used to describe such a behavior where the oscillation itself controls the phase with which the input of energy acts on it (for a recent review see Jenkins (2013)). This is completely different from the well-known phenomenon of forced resonance where the input is externally regulated through a driving force (such as $F_0 \cos \omega t$) and generates a maximum amplitude of oscillation when the driving frequency is tuned to match the natural frequency of the oscillator. It is interesting to note that self-oscillation is often misinterpreted as forced resonance even in popular physics textbooks (see Billah and Scanlan (1991)). Self-oscillation is usually the result of an instability of the linearized equation of motion for perturbations around an equilibrium, resulting in an oscillation whose amplitude grows exponentially with time until growth is inhibited by nonlinear effects (Jordan and Smith, 1987). This shows that rather than being mathematical curiosities, nonlinearities have a strong effect on the solutions of ordinary differential equations even when their magnitude is small.

3. Model behavior

The behavior of this nonlinear oscillator will be analyzed by numerically integrating its ordinary differential equation using an implicit Runge–Kutta method (e.g. Hairer and Wanner, 2010) subject to the following initial conditions: $t = 0, x = 0$ and $\dot{x} = v_{in}$. These conditions imply that a pressure variation originating near the orifice of the tube transfers momentum to the slug. The flow velocity towards the orifice is equal to the product of the speed of sound in the fluid c and the Mach number M of the flow. However, it has been shown experimentally that this flow velocity decreases by a factor $\phi = 0.35$ when the flow enters a narrow tube (James et al., 2006). The initial velocity of the slug will be $v_{in} = \phi \times c \times M$, where in order to fulfill the condition of incompressible flow the Mach number is set to a value significantly smaller than unity ($M = 0.01$). Even though this is an approximate way to estimate v_{in} , it should be noted that the choice of initial velocity does not affect the signal properties presented in later sections, but only the onset part of the synthetic waveform and its maximum amplitude.

As stated earlier, the linear dimension of the cavity ($L + h$) is limited by the fact that it should be much smaller than the wavelength of the pressure oscillations in the fluid. This means that for the fluids and frequency range (1–20 Hz) dealt with here this wavelength can vary from a few to tens of meters. Therefore the vertical length of the cavity is taken as $h = 0.5$ m and the length of the tube as $L = 0.1$ m. Two radius values are considered for the horizontal dimension of the cavity, one for a small cavity ($R = 0.35$ m) and another for a larger one ($R = 3$ m). In the former cavity it is expected that the nonlinear reaction force will be more significant due to the small volume involved, while in the latter one the nonlinear damping will be more influential due to the large difference in area cross-section for the tube and the cavity. The linear damping coefficient is inversely proportional to the tube's radius signifying that a small radius will contain boundary layers of comparable thickness to r and therefore viscous losses will increase. For example, if δ is calculated for steam (H_2O) as a function of r and for the two cavity sizes that are considered here, viscous losses increase significantly when r is smaller than 0.05 m

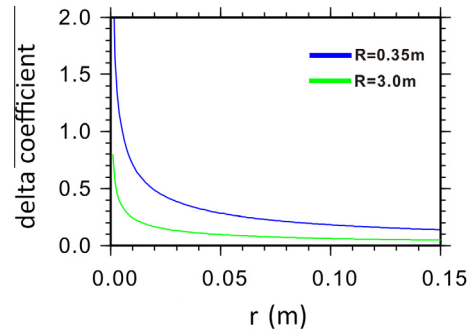


Fig. 3. Diagram showing the variation of the linear damping coefficient as a function of the tube's radius r , assuming that the fluid filling the cavity is pure steam (H_2O). The two curves correspond to two different cavity sizes as shown at the top right hand corner of the plot.

(Fig. 3). In order to avoid strong damping the radius of the tube is taken as $r = 0.07$ m which is a value reflecting small but not negligible viscous losses for both cavities ($\delta = 0.1–0.3$).

The slug displacement time series is calculated for different fluid compositions as the volume fraction of H_2O in gas mixtures and gas weight fraction in misty/dusty gases is increasing. The total signal duration, frequency of the dominant peak in the spectrum and the quality factor Q are then derived from the synthetic waveforms. In this study the quality factor is estimated as (Aki and Richards, 2002)

$$Q = \frac{f}{\Delta f} \quad (9)$$

where f is the peak frequency value and Δf is the bandwidth of the peak measured at one half its amplitude. The variation of these three parameters as a function of fluid composition is then considered and compared with observations. Figs. 4 and 5 show representative examples of synthetic waveforms for different fluid mixtures and for the two different values of R .

The kinds of fluid considered here cover the ones found in hydrothermal systems and volcanic conduits under a lithostatic pressure of 5 MPa. These fluids are gas mixtures such as H_2O+CO_2 and H_2O+SO_2 , as well as dusty and misty gases which are mixtures of SO_2 with fine ash particles and H_2O with water droplets respectively. In each case the fluid properties (viscosity, density, sound speed, specific heat ratio) are calculated following Kumagai and Chouet (2000) using the thermodynamic parameters compiled by the same authors. Gas mixtures are assumed to behave as ideal gases and there is no thermodynamic equilibrium between the gas and the liquid/solid phases. The temperature for the gas and the ash-gas mixtures is taken equal to 1200 K while for H_2O -water droplets mixture this value is taken as 584 K.

3.1. Gas mixtures

Total signal duration for both gas mixtures considered show only small variations as the volume of H_2O is increasing and range between 6 and 10 s for the small sized cavity while this range becomes 10 and 20 s for the large one (Fig. 6). The behavior of the dominant signal frequency seems to depend on the size of cavity radius. For the small cavity, the dominant signal frequency for both gas mixtures exhibits a peak at about 19 Hz for 0.3–0.4 volume fraction of H_2O . When the volume fraction becomes smaller or larger than this, dominant frequencies shift steadily to lower values and for fractions larger than 0.7 the two gas mixtures attain very similar frequency values. This is different from the case of a larger cavity where the dominant frequency for both mixtures varies in an almost linear fashion

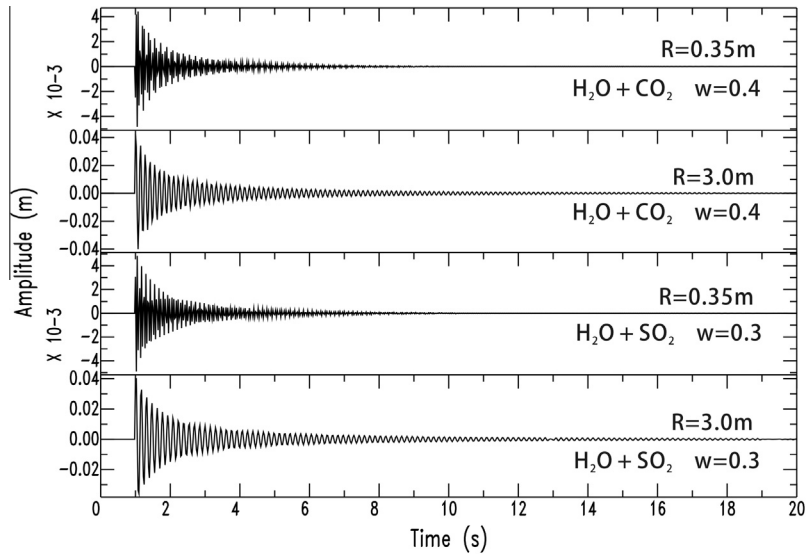


Fig. 4. Synthetic waveforms generated after integrating numerically the nonlinear ordinary differential equation (see text for more details) assuming that the fluid filling the cavity is a gas mixture. The cavity size, kind of gas mixture and volume fraction w of H_2O is shown at the right of each plot.

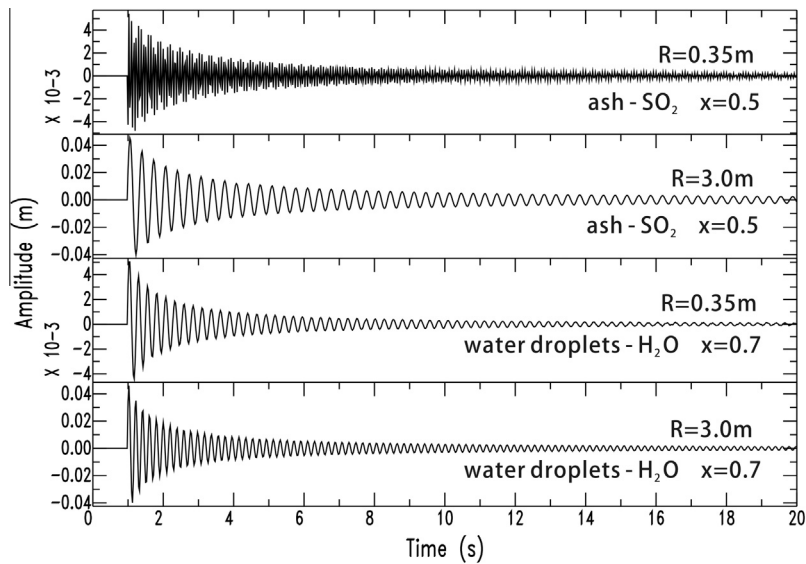


Fig. 5. Same as in Fig. 4 but this time the fluid filling the cavity is a gas-particle mixture. The symbol x is used to represent the gas weight fraction of SO_2 or H_2O in each plot. For clarity only the first 19 s of each waveform is shown.

as a function of volume fraction in the range between 4 and 10 Hz. In either case it is evident that the $\text{H}_2\text{O} + \text{CO}_2$ exhibits higher dominant frequencies than the $\text{H}_2\text{O} + \text{SO}_2$ mixture when the volume fraction of H_2O is smaller than 0.4. The quality factors of the synthetic signals show a greater variability for the small cavity, since they assume values between 4 and 45 while there is a decreasing trend for both gas mixtures as the volume fraction of H_2O increases. Fluctuations are smaller for the large cavity and Q values vary over a limited range between 28 and 45 showing an increase as the volume fraction becomes larger. Such quality factors are similar in magnitude to those obtained for the fluid-driven crack model for different gas mixtures by Kumagai and Chouet (2000). Amplitude modulation effects can be seen in synthetic signals corresponding to the small cavity for 0.3–0.4 volume fraction of H_2O (cf. Fig. 4).

3.2. Gas-particle mixtures

As in Kumagai and Chouet (2000) the sound speeds and density for the different gas-particle mixtures are calculated for volume fractions of pure gas larger than 0.5, which corresponds to fluids with more than 2 wt.% of pure gas at a temperature of 1200 K. It is also assumed that the radius of the individual particles (either ash or water droplets) is $1 \mu\text{m}$. Signal durations for either the small or large cavity exhibit a trend of decreasing values as the gas weight fraction increases (Fig. 7). Largest durations are observed for dusty gas mixtures with maximum values of 55 and 118 s corresponding to the small and large cavity respectively. Mixtures of ash and SO_2 seem to exhibit larger signal durations than the mixtures of H_2O and water droplets. Also there is a small decrease in duration when the gas weight fraction in dusty gas falls below

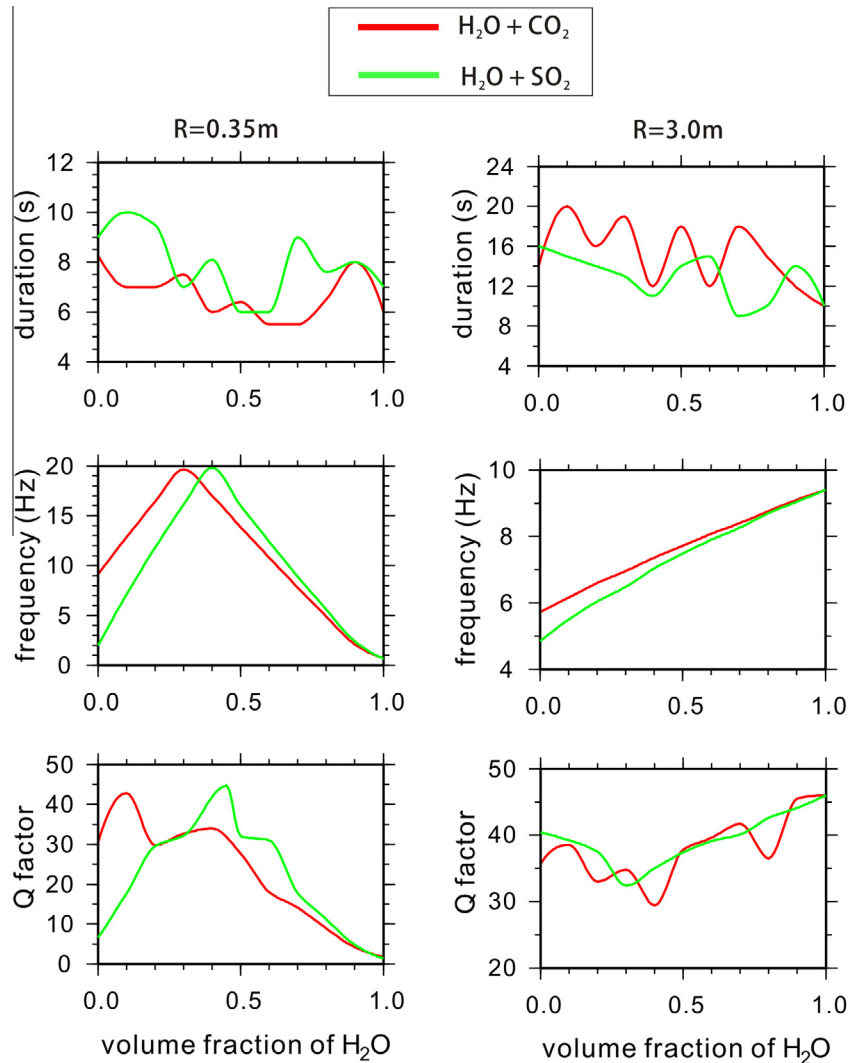


Fig. 6. Diagrams summarizing the signal characteristics when the fluid in the cavity is a gas mixture. Left panel: variation of signal duration, dominant frequency and quality factor as a function of volume fraction of H₂O for a cavity with radius $R = 0.35$ m. Right panel: the same for a cavity with radius $R = 3.0$ m.

0.2 and the mixture becomes rich in ash particles. Similar to the case of gas mixtures, the behavior of dominant frequency is different between small and the large cavity. For the small cavity both mixtures reach a maximum dominant frequency (18–19 Hz) for low gas weight fractions (0.2–0.3), while for larger fractions frequencies decrease steadily. The two mixtures also behave differently when the gas fraction becomes larger than 0.5; the frequency of ash-SO₂ continues to decrease until it stabilizes to a value of 1–2 Hz for 0.9–1.0 gas weight fraction. On the other hand, the frequency curve for the water droplets-H₂O reaches a minimum for 0.6 gas weight fraction increasing up to 16 Hz for larger fraction values. When the cavity becomes large the frequency increases smoothly for both mixtures from 1 to 7 Hz as the gas weight fraction becomes larger.

For the small cavity the quality factors mirror the variations in dominant frequency with the ash-SO₂ mixtures exhibiting the largest values compared to those of water droplets-H₂O. An increasing fraction of SO₂ progressively lowers the Q values enhancing the attenuation of the synthetic signal. Quality factors for the water droplets-H₂O mixtures follow initially the same trend of decreasing values up to a gas weight fraction of 0.6, however, after this they increase again up to a value of 60. Amplitude modulation can also be seen for both types of mixtures when the gas weight fraction is below 0.5. The quality factors for the large

cavity remain high and do not show the same decreasing trend as for the small cavity. In the case of ash-SO₂ they reach a maximum value of 180 and then stabilize to a value around 60 for 0.4–0.9 gas weight fractions. An interesting characteristic is that for both cavity sizes the Q values exhibit a significant drop when the gas weight fraction falls below 0.2 and is enriched in ash particles. For the water droplets-H₂O mixture the Q values appear almost constant around 60 for low gas weight fractions fluctuating between 50 and 140 when the gas contribution becomes higher than 0.4. These results regarding cavities agree rather well with those of Kumagai and Chouet (2000) that gas-particle mixtures inside a crack can cause long-lasting oscillations with Q values of several hundred.

4. Comparison with observations at Galeras

The eruptive activity of Galeras volcano started during February 1989 when small ash and gas emissions occurred and were followed by similar emissions during May of the same year and August 1990 (Cortés and Raigosa, 1997). These small eruptive episodes were accompanied by mild seismic activity in the form of volcano-tectonic and long-period events, as well as volcanic tremor. At the end of 1990 deformation observations indicated

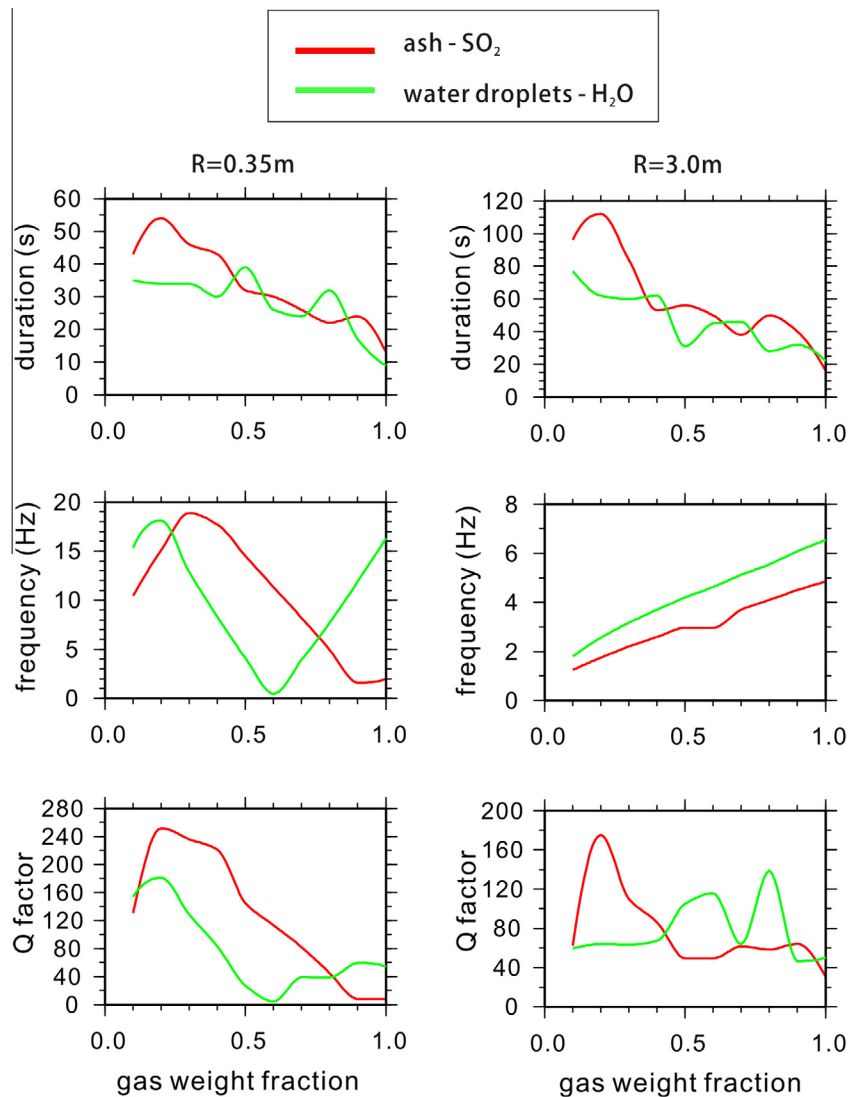


Fig. 7. Same as in Fig. 5 when the fluid filling the cavity is a gas-particle mixture.

inflationary behavior accompanied by an increasing number of long-period events, bursts of volcanic tremor and minor gas emissions. This activity intensified in October 1991 with the emplacement and extrusion of an andesitic lava dome at the base of the main crater. After November 1991 the long-period seismicity declined sharply until mid-July 1992 when the first tornillo events appeared and were followed by an eruption that destroyed the uppermost part of the dome. Five more vulcanian eruptions occurred in January, March, April (4th and 13th) and June 1993 of which four of them were preceded by tornillo events. Measurements of SO₂ flux using correlation spectroscopy revealed that the gas emission steadily decreased during the period prior to every eruption, increasing again afterwards (Fisher et al., 1994; Stix et al., 1997; Zapata et al., 1997). Such a pattern supports the interpretation that the volcanic conduits were obstructed leading to the pressurization of the system and to explosive activity. Each eruptive cycle between July 1992 and June 1993 was associated with a series of seismic phenomena that first started with tornillo signals, then high-frequency but short duration events called 'mariposas' followed by explosive activity and a swarm of long-period events (Cortés and Raigosa, 1997; Zapata et al., 1997; Gil-Cruz and Chouet, 1997).

4.1. Tornillos waveform characteristics

There are two main physical quantities whose variations have been studied in detail during the 1992–1993 eruptive activity at Galeras, namely signal duration and oscillation quality factors. These observations and their consistency with the cavity model are summarized as follows:

- Before each eruptive cycle tornillo signals exhibited an increasing signal duration that was followed by a decrease just before the onset of the eruption (Narváez et al., 1997; Gómez and Torres, 1997; Gómez et al., 1999). This characteristic has been highlighted in all studies of tornillos occurring at Galeras during 1992–1993 as a tool to forecast eruptive activity. It is interesting that the cavity model proposed here can reproduce this observation: when the SO₂-ash mixture filling the cavity is reaching a gas weight fraction of 0.2 (i.e. it is enriched in ash) the signal duration indeed drops (cf. Fig. 7).
- Gómez et al. (1999) calculated damping coefficients ($=1/2Q$) for all tornillos that occurred at Galeras between 1992 and 1995 and found that these range between 0.002 and 0.016. The lowest and highest Q factors of synthetic tornillos for the large

cavity filled with ash-SO₂ mixture, are 35 and 180 respectively (cf. Fig. 7). The damping coefficients that correspond to these values are 0.014 and 0.002 respectively, in good agreement with the observations.

The previous studies also noticed a temporal variation of the dominant frequency of tornillos, shifting from about 4 Hz and stabilizing to around 1 Hz prior to each eruption. In the context of the cavity model this observation can be explained as the result of a changing fluid composition to a SO₂-ash mixture that is enriched in ash as the eruption is approaching. The frequency of 4 Hz corresponds to a gas weight fraction of 0.7 while for a gas weight fraction of 0.1 the signal frequency becomes about 1 Hz (cf. Fig. 7). Obviously, these frequency variations can be explained without invoking any sharp changes in the geometry or size of the cavity.

4.2. Reduced displacement of tornillos

A quantity that is utilized in order to infer the strength of the seismic source of volcano-seismic signals is that of reduced displacement (Aki and Koyanagi, 1981; Fehler, 1983). It has units of distance multiplied by displacement amplitude (usually given in cm²) and can be calculated using the following equation if the wavefield consists of body waves

$$D_R = \frac{A}{2\sqrt{2}} \frac{d}{G} \quad (10)$$

while if it consists of surface waves the equation becomes

$$D_R = \frac{A}{2\sqrt{2}} \frac{\sqrt{d\lambda}}{G} \quad (11)$$

where A is the displacement amplitude of the signal, d is the source-receiver distance, G is the instrument magnification and λ is the wavelength. In order to estimate displacement amplitudes for tornillos the following procedure is used: Narváez et al. (1997) provide maximum peak amplitudes v_p (in $\mu\text{m/s}$) of tornillos, recorded at station 'Cráter-2' ($d = 1.6$ km), for each of the four eruptive phases during 1992–1993 along with their corresponding periods (Table 2). The amplitude envelope of tornillos at Galeras consists of two parts, namely an excitation function where the amplitude increases exponentially towards the peak value, and a response function where amplitudes decay exponentially. In particular, Seidl et al. (1999) approximated the excitation function of tornillos as

$$v = v_p(1 - e^{-qt}) \quad (12)$$

where the coefficient q depends on the rise time t_R . From the 13 tornillo types shown in Fig. 3(a–m) of Narváez et al. (1997) the rise time can be estimated with reasonable accuracy (± 1 s) and it is found to have a minimum value of 2 s and a maximum of 5 s. Eq. 12 is then integrated for these two values and for each value of v_p so as to obtain displacement A . The calculation of instrument magnification G for each of the observed periods of tornillos is outlined in Appendix B. The seismic wavefield of tornillos at Galeras is quite complicated in part due to the rough topography, however,

Table 2

Summary of maximum peak velocity amplitudes (v_p) and corresponding periods T for tornillo events recorded at Galeras during the four inter-eruptive periods (from Narváez et al. (1997)). The two columns of reduced displacement D_R are estimated for each period using two rise time (t_R) values (see text for more details).

Period	v_p (m s ⁻¹)	T (s)	($t_R=2$ s) D_R (cm ²)	($t_R=5$ s) D_R (cm ²)
July 1992	23×10^{-6}	0.8	1.97	4.75
January 1992	31×10^{-6}	0.8	2.66	6.40
February 1993	27×10^{-6}	0.4	1.50	3.62
April 1993	10×10^{-6}	0.6	0.70	1.68

the rather shallow source depth (<1 km) implies it may predominantly consist of surface waves (Gómez et al., 1999). Taking then the phase velocity $C = 0.9\beta$ with shear wave velocity $\beta = 1500$ m/s for wavelength calculation, D_R is estimated and the results are summarized in Table 2.

The question that naturally arises is whether a cavity size of $h = 0.5$ m and $R = 3.0$ m can produce similar reduced displacements as the ones estimated previously. Synthetic reduced displacement sD_R can be calculated by assuming a semi-infinite medium and a wavefield consisting of the fundamental mode of Rayleigh waves, as (Aki and Richards, 2002; Chouet, 1996; McNutt and Nishimura, 2008)

$$sD_R = \sqrt{\frac{2r(d)}{8CUI_1}} (1.23e^{-0.85Kz} - 0.58e^{-0.39Kz}) (\pi h R^2 \Delta P) \quad (13)$$

where $r(d)$ is the fundamental mode of the eigenfunction, C is phase velocity, U is group velocity (here taken as $U = C = 0.9\beta$), I_1 is the energy integral, K the wavenumber, z is the source depth and ΔP is the overpressure inside the cavity. This equation also assumes that the moment tensor describing the seismic source is dominated by a volumetric component resulting in the off-diagonal elements being equal to zero. The calculations are performed for the three periods (0.4, 0.6, 0.8 s) of observed maximum amplitudes and three trial depths (100, 200 and 300 m); shear wave velocity is taken as $\beta = 1500$ m/s while rock density as $\rho_s = 2100$ kg/m³. Theoretically overpressure within domes can take values of tens of MPa, in practice however, leakage of fluids to the surrounding rocks limits considerably its value (Sparks, 1997) therefore here it is assumed that $\Delta P = 1$ MPa.

Fig. 8 shows the variation of sD_R as a function of distance from the source for each observed period at each trial depth. The best agreement between observed and synthetic reduced displacement can be found for $z = 200$ m. At this depth and for $d = 1.6$ km, sD_R is within/close to the range of D_R values for observed periods 0.4 s ($sD_R = 2.10$ cm²) and 0.6 s ($sD_R = 1.72$ cm²). This is not the case for the observed period of 0.8 s where sD_R has a value of 14.86 cm² that is outside the range of estimated D_R . However, if the source depth is taken as 250 m then sD_R becomes 5.20 cm² which is within the estimated range. As the period of 0.8 s corresponds the maximum amplitude of tornillos during the first two phases of activity (cf. Table 2), this implies that at that time the source might have been slightly deeper. Temporal variations of overpressure from one eruptive phase to the next may also explain the range of D_R values. It is worth mentioning that the sD_R curves show that the 0.8 s period produces very small reduced displacement beyond a distance of 4 km when the depth is less than 300 m. This agrees well with the distance range where tornillos are usually observed (cf. Table 1). The cavity depth of 200–250 m derived here corresponds to the lower part of the dome and lies above the inferred point deformation source (~ 350 m) associated with the extrusion of the dome (Gil-Cruz and Chouet, 1997).

5. Discussion

5.1. What are the losses due to seismic energy radiation?

As the lumped parameter model does not consider coupling of the fluid-cavity system to the rock, an issue that should be addressed is whether the oscillator losses due to radiation of seismic energy are significant or not. Chouet (1985) has considered this problem in a similar context, where a fluid-filled cylinder of length h and radius R is subject to an oscillatory fluid motion. The coefficient that expresses the partitioning of energy into elastic and hydraulic motions can be approximated for the disk-shaped end of the cylinder as

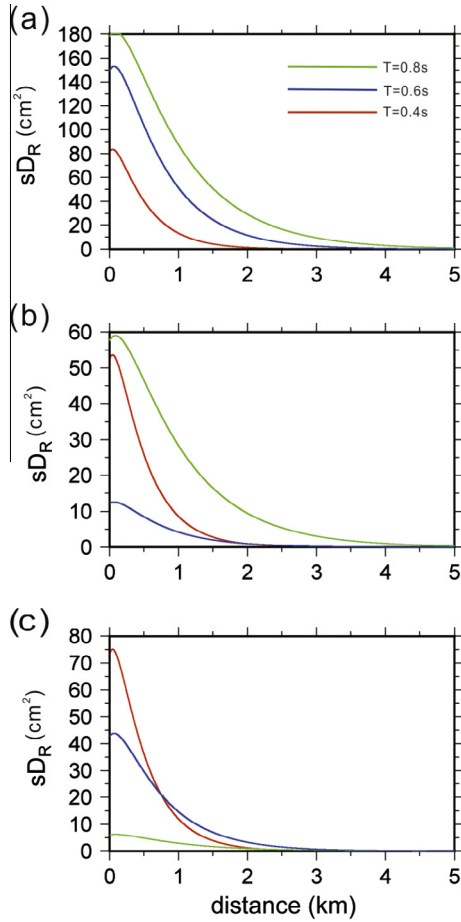


Fig. 8. Diagrams showing the variation of synthetic reduced displacement (sD_R) as a function of distance from the source. Calculations assume a cavity with $R = 3$ m, $L = 0.5$ m, wave periods 0.4 s, 0.6 s, 0.8 s and a source depth of (a) 100 m, (b) 200 m, (c) 300 m.

$$\eta_{disk} = 0.3 \frac{\omega \pi R}{\alpha} \quad (14)$$

where $\omega = 2\pi f$ and α is the compressional wave speed. The partitioning coefficient for the cylinder itself was approximated by

$$\eta_{cyl} = 0.08 h R^2 \left(\frac{\omega}{\beta}\right)^3 \quad (15)$$

where $\beta (= 1500 \text{ m/s})$ is shear wave speed and it is assumed that the rock is a Poisson solid with $\alpha/\beta = \sqrt{3}$. For the cavity size of $h = 0.5$ m and $R = 3$ m and the frequency range observed at Galeras (1–4 Hz) the coefficient η_{disk} takes values between 0.006 and 0.027 while η_{cyl} is far smaller in the order of 10^{-6} . It can be concluded that only a small fraction of the hydraulic motion is converted into seismic energy radiation for this frequency range. One criticism against such calculations would be that the cavity geometry at Galeras may be quite different from cylindrical. Fujita and Ida (2003) have formulated the normal mode patterns for three simple geometrical shapes (plane, cylinder and sphere) and tried to distinguish the shape of volcanic fluid systems at different volcanoes based on these patterns. Specifically, at Galeras the authors concluded that the normal mode pattern suggests a cylindrical shaped source.

5.2. Is the cavity model consistent with source inversion results?

Even though (to the best knowledge of the author) there is no published study dealing with source inversion of the Galeras tornillos, it would still be interesting to compare the physical model introduced here with such results obtained for tornillos from

Kusatsu-Shirane volcano in Japan. Nakano et al. (2003) investigated the source process of these events by waveform inversion of their effective excitation functions (i.e. the apparent excitation observed at individual receivers). In this way, the authors were able to determine the source-time functions of the six moment tensor elements, as well as three single force components (F_x, F_y, F_z) that were required in order to fit the waveform data. The results point to a process where fluid movement occurs in a nearly vertical direction and the source region is compressed and dilated in cycles as indicated by the oscillatory nature of the time history of the force components and the M_{xx}, M_{yy}, M_{zz} moment elements. This kind of inversions have the limitation that they can only determine the relative amplitudes of moment elements/force components and cannot decipher the exact dimensions of the source region. However, the source process described by Nakano et al. (2003) is not in conflict with the proposed fluid-filled cavity model where upward and downward forces also cause volumetric changes to the cavity.

5.3. Is there a physical basis for the cavity model?

Stix et al. (1997) observed a positive correlation between the length of quiescence from one eruption to the next and the number of post-eruptive long-period events at Galeras. On the other hand, they also observed a negative correlation for the post-eruptive seismicity and the number of days over which the tornillo events occurred. The authors finally concluded about the timescale of gas exsolution and accumulation that:

These data suggest a model of progressive gas accumulation over a period of months between eruptions, rather than rapid pressurization and sealing of the conduit days to weeks before an eruption. The appearance of monochromatic signals before an eruption may therefore be an indication of a pressurization threshold in the conduit being exceeded, rather than a manifestation of the beginning of a pressurization episode.

This conclusion succinctly highlights two crucial points related to the generation of tornillo events. First, that the gas accumulation was not sudden or episodic but rather a slow and nearly steady process. Second, that tornillo events might have been triggered after a fluid pressure threshold was exceeded. Both of these points are consistent with the self-oscillations of a fluid filling a cavity: the steady accumulation of fluid leads to a critical point when excess fluid tries to enter the cavity but is being repelled by the high pressure gradient. In this way the nearly steady input of fluid is transformed into the oscillatory motion of the slug.

Tornillos are usually observed at volcanoes that possess extensive hydrothermal systems, with prominent examples being Vulcano in Italy and Tongariro in New Zealand. In these settings the chemical and mechanical action of hydrothermal fluids to the host rocks may cause the formation of cavities at shallow depths and the steady accumulation of fluids within these cavities. The precipitation of hydrothermal minerals in the cracks surrounding these cavities may then lead to sealing and subsequent buildup of fluid pressure (see for example Fournier (2006)) until a critical value is reached and fluid oscillatory motion starts.

Acknowledgments

I would like to thank the Ministry of Science and Technology (MOST) of Taiwan for the financial support of this research. Mark Jellinek and Robin Matoza provided thoughtful reviews that improved the original manuscript. I am also grateful to Elias Koutsoukos for his advice on how to estimate instrument magnification and corresponding displacements of the Galeras tornillos.

Appendix A

It is possible to derive the nonlinear ordinary differential equation that governs the behavior of the fluid filled cavity oscillator by considering Newton's second law and all relevant forces in the form

$$\Sigma F = F_v + F_r + F_d = m\ddot{x} \quad (A1)$$

where F_v is the viscous damping force, F_r is the reaction force of the fluid within the cavity and F_d is the nonlinear damping force exerted on the fluid slug. Each of these forces are given by

$$F_v = -2\delta m\dot{x} \quad (A2)$$

$$F_r = -\left(\frac{\rho_f c^2 s^2}{V}\right) \left[x - \frac{1}{2}(\gamma + 1) \left(\frac{s}{V}\right) x^2 + \dots \right] \quad (A3)$$

$$F_d = \left(\frac{1}{2}\rho_f \zeta s\right) \dot{x}^2 = \left(\frac{1}{2}\rho_f \zeta s\right) \dot{x}|\dot{x}| \quad (A4)$$

Substituting these terms back to eq. A1 and dividing both parts by the mass of the slug ($m = \rho_f L_e s$) also ignoring higher order contributions yields

$$-2\delta\ddot{x} - \frac{c^2 s}{L_e V} \left[x - \frac{1}{2}(\gamma + 1) \left(\frac{s}{V}\right) x^2 \right] + \frac{\zeta}{2L_e} \dot{x}|\dot{x}| = \ddot{x} \quad (A5)$$

After re-arranging the terms and recognizing that $\omega_0^2 = \frac{c^2 s}{L_e V}$ will yield the final nonlinear ordinary differential equation which is

$$\ddot{x} + 2\delta\ddot{x} + \frac{\zeta}{2L_e} |\dot{x}|\dot{x} + \omega_0^2 \left[x - \frac{1}{2}(\gamma + 1) \left(\frac{s}{V}\right) x^2 \right] = 0 \quad (A6)$$

Appendix B

The tornillo signals at station 'Cráter-2' have been recorded by a vertical component Sprengner instrument with a natural period of 1.0 s and damping coefficient 0.72 (critical) (Narváez et al., 1997). The magnification of such an instrument can be calculated by the relationship (e.g. Papazachos et al., 2005)

$$G = \frac{1}{\sqrt{\left(1 - \frac{T^2}{T_0^2}\right)^2 + \frac{4\zeta^2 T^2}{T_0^2}}} \quad (B1)$$

where T is the period of the observed wave, T_0 is the natural period of the seismometer and ζ is its damping coefficient. For the observed periods of tornillos at 0.8 s, 0.6 s, 0.4 s the value of G is 0.83, 0.93 and 0.98 respectively.

References

- Aki, K., Koyanagi, R.Y., 1981. Deep volcanic tremor and magma ascent mechanism under Kilauea, Hawaii. *J. Geophys. Res.* 86, 7095–7110.
- Aki, K., Richards, P.G., 2002. *Quantitative Seismology*. University Science Books.
- Alparone, S., Cannata, A., Gambino, S., Gresta, S., Milluzzo, V., Montalto, P., 2010. Time-space variation of volcano-seismic events at La Fossa (Volcano, Aeolian Islands, Italy): new insights into seismic sources in a hydrothermal system. *Bull. Volcanol.* 72, 803–816. <http://dx.doi.org/10.1007/s00445-010-0367-6>.
- Batchelor, G.K., 1967. *An Introduction to Fluid Dynamics*. Cambridge University Press.
- Billah, K.Y., Scanlan, R.H., 1991. Resonance, Tacoma Narrows bridge failure and undergraduate physics textbooks. *Am. J. Phys.* 59, 118–124.
- Bouloso, R.R., Bustamante, F.-O., 1992. The reaction force on a Helmholtz resonator driven at high sound pressure amplitudes. *Am. J. Phys.* 60, 722–726.
- Chouet, B.A., 1985. Excitation of a buried magmatic pipe: a seismic source model for volcanic tremor. *J. Geophys. Res.* 90, 1881–1893.

- Chouet, B.A., 1996. New methods and future trends in seismological volcano monitoring. In: Scarpa, Tilling (Eds.), *Monitoring and Mitigation of Volcano Hazards*. Springer, pp. 23–97.
- Cortés, G.P., Raigosa, J., 1997. A synthesis of the recent activity of Galeras volcano, Colombia: seven years of continuous surveillance, 1989–1995. *J. Volcanol. Geotherm. Res.* 77, 101–114.
- De Angelis, S., 2006. Analyses of unusual long-period earthquakes with extended coda recorded at Katmai National Park, Alaska, USA. *Geophys. Res. Lett.* 33, L07306. <http://dx.doi.org/10.1029/2005GL025581>.
- Fehler, M., 1983. Observations of volcanic tremor at Mt. St. Helens volcano. *J. Geophys. Res.* 88, 3476–3484.
- Fisher, T.P., Morrissey, M.M., Calvache, M.L., Gómez, D., Torres, R., Stix, J., Williams, S.N., 1994. Correlations between SO_2 flux and long-period seismicity at Galeras volcano. *Nature* 368, 135–137.
- Fournier, R.O., 2006. Hydrothermal systems and volcano geochemistry. In: Dzurisin, D (Ed.), *Volcano Deformation: Geodetic Monitoring Techniques*. Springer, pp. 323–341.
- Fujita, E., Ida, Y., 2003. Geometrical effects and low-attenuation resonance of volcanic fluid inclusions for the source mechanism of long-period earthquakes. *J. Geophys. Res.* 108, 2118. <http://dx.doi.org/10.1029/2002JB001806>.
- Gil-Cruz, F., Chouet, B.A., 1997. Long-period events, the most characteristic seismicity accompanying the emplacement and extrusion of a lava dome in Galeras volcano, Colombia, in 1991. *J. Volcanol. Geotherm. Res.* 77, 121–158.
- Gómez, D.M., Torres, R.A., 1997. Unusual low-frequency volcanic seismic events with slowly decaying coda waves observed at Galeras and other volcanoes. *J. Volcanol. Geotherm. Res.* 77, 173–193.
- Gómez, D.M., Torres, R.A., Seidl, D., Hellweg, M., Radenmacher, H., 1999. Tornillo seismic events at Galeras volcano, Colombia: a summary and new information from broadband three-component measurements. *Ann. Geophys.* 42, 365–378.
- Hagerty, M., Benites, R., 2003. Tornillos beneath Tongariro Volcano, New Zealand. *J. Volcanol. Geotherm. Res.* 125, 151–169. [http://dx.doi.org/10.1016/S0377-0273\(03\)00094-5](http://dx.doi.org/10.1016/S0377-0273(03)00094-5).
- Hairer, E., Wanner, G., 2010. *Solving Ordinary Differential Equations II: Stiff and Differential Algebraic Problems*. Springer.
- Hamada, N., Jingu, H., Ikumoto, K., 1976. On the volcanic earthquakes with slowly decaying coda wave. *Bull. Volcanol. Soc. Jpn.* 21, 167–183.
- Howe, M.S., 1976. On the Helmholtz resonator. *J. Sound Vib.* 45, 427–440.
- James, M.R., Lane, S.J., Chouet, B.A., 2006. Gas slug ascent through changes in conduit diameter: laboratory insights into a volcano-seismic source process in low-viscosity magmas. *J. Geophys. Res.* 111, B05201. <http://dx.doi.org/10.1029/2005JB003718>.
- Jenkins, A., 2013. Self-oscillation. *Phys. Reports* 525, 167–222. <http://dx.doi.org/10.1016/j.physrep.2012.10.007>.
- Jordan, D.W., Smith, P., 1987. *Nonlinear Ordinary Differential Equations*. Oxford University Press.
- Kumagai, H., Chouet, B.A., 2000. Acoustic properties of a crack containing magmatic or hydrothermal fluids. *J. Geophys. Res.* 105, 25493–25512.
- Kumagai, H., Chouet, B.A., Nakano, M., 2002. Waveform inversion of oscillatory signatures in long-period events beneath volcanoes. *J. Geophys. Res.* 107, 2301. <http://dx.doi.org/10.1029/2001JB001704>.
- Kumagai, H., Chouet, B.A., Nakano, M., 2002. Temporal evolution of a hydrothermal system in Kusatsu-Shirane volcano, Japan, inferred from the complex frequencies of long-period events. *J. Geophys. Res.* 107, 2236. <http://dx.doi.org/10.1029/2001JB000653>.
- Lesage, P., Surono, 1995. Seismic precursors of the February 10, 1995 eruption of Kelut volcano, Java. *J. Volcanol. Geotherm. Res.* 65, 135–146.
- McNutt, S.R., Nishimura, T., 2008. Volcanic tremor during eruptions: temporal characteristics, scaling and constraints on conduit size and processes. *J. Volcanol. Geotherm. Res.* 178, 10–18. <http://dx.doi.org/10.1016/j.jvolgeores.2008.03.010>.
- Milluzzo, V. et al., 2010. Tornillos at Vulcano: clues to the dynamics of the hydrothermal system. *J. Volcanol. Geotherm. Res.* 198, 377–393. <http://dx.doi.org/10.1016/j.jvolgeores.2010.09.022>.
- Molina, I., Kumagai, H., Yepes, H., 2004. Resonances of a volcanic conduit triggered by repetitive injections of an ash-laden gas. *Geophys. Res. Lett.* 31, L03603. <http://dx.doi.org/10.1029/2003GL018934>.
- Nakano, M., Kumagai, H., 2005. Response of a hydrothermal system to magmatic heat inferred from temporal variations in the complex frequencies of long-period events at Kusatsu-Shirane volcano, Japan. *J. Volcanol. Geotherm. Res.* 147, 233–244. <http://dx.doi.org/10.1016/j.jvolgeores.2005.04.003>.
- Nakano, M., Kumagai, H., Chouet, B.A., 2003. Source mechanism of long-period events at Kusatsu-Shirane volcano, Japan, inferred from waveform inversion of the effective excitation functions. *J. Volcanol. Geotherm. Res.* 122, 149–164.
- Narváez, L., Torres, R.A., Gómez, D.M., Cortés, G.P., Cepeda, H., Stix, J., 1997. 'Tornillo'-type seismic signals at Galeras volcano, Colombia, 1992–1993. *J. Volcanol. Geotherm. Res.* 77, 159–171.
- Papazachos, B., Karakaisis, G.F., Hatzidimitriou, P.M., 2005. *Introduction to Seismology* (in Greek). Ziti editions, Thessaloniki.
- Rienstra, S.W., Hirschberg, A., 2004. *An Introduction to Acoustics*. Eindhoven University of Technology.
- Seidl, D., Hellweg, M., 2003. Parameterization of multichromatic tornillo signals observed at Galeras volcano (Colombia). *J. Volcanol. Geotherm. Res.* 125, 171–189. [http://dx.doi.org/10.1016/S0377-0273\(03\)00095-7](http://dx.doi.org/10.1016/S0377-0273(03)00095-7).

- Seidl, D., Hellweg, M., Radenmacher, H., Gómez, D.M., Torres, R.A., 1999. The anatomy of a tornillo: puzzles from three-component measurements at Galeras volcano (Colombia). *Ann. Geophys.* 42, 355–364.
- Sparks, R.S.J., 1997. Causes and consequences of pressurisation of lava dome eruptions. *Earth Planet Sci. Lett.* 150, 177–189.
- Stix, J., Torres, R., Narváez, L., Cortés, G.P., Raigosa, J., Gómez, D., Castonguay, R., 1997. A model of vulcanian eruptions at Galeras volcano, Colombia. *J. Volcanol. Geotherm. Res.* 77, 285–303.
- Zapata et al., 1997. SO₂ fluxes from Galeras volcano, Colombia, 1989–1995: progressive degassing and conduit obstruction of a decade volcano. *J. Volcanol. Geotherm. Res.* 77, 195–208.